INTERNATIONAL JOURNAL FOR NUMERICAL METHODS IN FLUIDS
Int. J. Numer. Meth. Fluids 2001; **36**: 885–902 (DOI: 10.1002/fld.150)

Finite volume multigrid method of the planar contraction flow of a viscoelastic fluid

H. Al Moatssime[a], D. Esselaoui[b], A. Hakim[a] and S. Raghay[a,*]

[a] *Université Cadi Ayyad, Faculté des Sciences et Techniques, Département de Maths Info, B.P. 618, Guéliz Marrakech, Morocco*
[b] *Laboratoire des Sciences de l'Ingénieur, Analyse Numérique et Optimisation, Université Ibn Tofail, Kénitra, Morocco*

SUMMARY

This paper reports on a numerical algorithm for the steady flow of viscoelastic fluid. The conservative and constitutive equations are solved using the finite volume method (FVM) with a hybrid scheme for the velocities and first-order upwind approximation for the viscoelastic stress. A non-uniform staggered grid system is used. The iterative SIMPLE algorithm is employed to relax the coupled momentum and continuity equations. The non-linear algebraic equations over the flow domain are solved iteratively by the symmetrical coupled Gauss–Seidel (SCGS) method. In both, the full approximation storage (FAS) multigrid algorithm is used. An Oldroyd-B fluid model was selected for the calculation. Results are reported for planar 4:1 abrupt contraction at various Weissenberg numbers. The solutions are found to be stable and smooth. The solutions show that at high Weissenberg number the domain must be long enough. The convergence of the method has been verified with grid refinement. All the calculations have been performed on a PC equipped with a Pentium III processor at 550 MHz. Copyright © 2001 John Wiley & Sons, Ltd.

KEY WORDS: FAS multigrid algorithm; FVM; non-uniform staggered grid; Oldroyd-B fluid; SIMPLE algorithm

1. INTRODUCTION

Polymeric fluids are of particular interest in the numerical simulation community because of their wide applications in materials processing, for example, extrudation of polymers through dyes. Their behavior is different from that of Newtonian fluids in ways that are often complex and striking.

Flow of non-Newtonian materials through abrupt contractions, the stick–slip problem, and the extrudate swell have been designated the most important problems for both experimentalists and numerical analysts.

* Correspondence to: Université Cadi Ayyad, Faculté des Sciences et Techniques, Département de Maths Info, B.P. 618, Guéliz Marrakech, Morocco.

Received May 2000
Revised November 2000

The first numerical simulations of flows of viscoelastic fluids have only found limited use in view of a reduced range of Weissenberg numbers. This phenomena is called the 'high-Weissenberg number problem' (Reference [1], chapter 11). The cause of the failure of these numerical simulations is purely numerical: the mixed elliptic–hyperbolic nature of the equations, geometrical singularities (corner of the abrupt contraction, stick–slip transition), large stress concentration, etc.

Many numerical methods have been used and a variety of results have been produced. Early attempts were based on the finite difference method [2]. In recent years, successful finite element methods have emerged. For instance, Marchal and Crochet [3] developed a new mixed finite element method. This method permits the simulation of the flows of upper convected Maxwell and Oldroyd-B fluids at rather high values of the Weissenberg number. Their numerical scheme introduced an element which has a 4×4 subdivision of the element for stress and an artificial diffusion by non-consistent streamline upwind (SU) for discretizing the constitutive equation. King *et al.* [4] and Bindette *et al.* [5] developed an explicitly elliptic momentum equation (EEME). Rajagopalan *et al.* [7] proposed an elastic–viscous split-stress finite element method coupled with the streamline upwind Petrov–Galerkin (SUPG) method for the viscoelastic flow system. Another approach is a combined pseudo-spectral/finite element method developed by Beris *et al.* [6]. Fortin and Fortin [9] simulated the flow through the 4:1 planar contraction of an Oldroyd-B fluid by using the SU technique and the Lesaint–Raviart method, and they obtained solutions at high Weissenberg numbers. In 1990, Fortin and Fortin [10] solved the stick–slip flow of an Oldroyd-B fluid by using an iterative method based on the generalized minimal residual (GMRES) method; they obtained solutions for moderate Weissenberg numbers. Later, Fortin and Zine [8] redefined an extra-stress tensor and improved the range of convergence.

The finite volume method (FVM) has gradually been used more within the viscoelastic context [11–14], since this method has been used successfully in other fields of computational fluid mechanics. Raghay and Hakim [15] have developed an FVM for solving the White Metzner fluid in 4:1 planar contraction.

In this paper we are interested in the introduction of the multigrid method [full approximation storage (FAS)] and a comparison of CPU between the single grid and multigrid algorithm using a family of meshes. For calculations we have selected the Oldroyd-B model on the 4:1 planar contraction. First we state the governing equations for the Oldroyd-B fluid and we give the boundary conditions for the planar 4:1 contraction. In Section 3 we describe the finite volume approximations of the governing equations and boundary conditions. A multigrid method (FAS) will be presented. Numerical results are presented in the last section.

2. MATHEMATICAL MODELING

2.1. Fluid flow equations

We consider an incompressible flow of a viscoelastic fluid. The movement is governed by the dynamic equilibrium and the mass conservation, while fluid behavior is described by the Oldroyd-B constitutive equation

$$\rho \frac{\partial \underline{U}}{\partial t} + \rho(\underline{U} \cdot \nabla)\underline{U} = \operatorname{div} \underline{\underline{\tau}} \tag{1}$$

$$\operatorname{div} \underline{U} = 0 \tag{2}$$

$$\underline{\underline{\tau}} + \lambda_1 \frac{\mathrm{D}_a \underline{\underline{\tau}}}{\mathrm{D}t} = 2\eta \left(\underline{\underline{D}} + \lambda_2 \frac{\mathrm{D}_a \underline{\underline{\tau}}}{\mathrm{D}t} \right) \tag{3}$$

where $\underline{\underline{\tau}}$ is the extra-stress tensor; $\underline{\underline{D}}$ is the strain rate tensor, $\underline{\underline{D}} = \frac{1}{2}(\nabla \underline{U} + (\nabla \underline{U})^T)$; λ_1 and λ_2 are the relaxation time and retardation time respectively; and η is the field viscosity.

The operator $\mathrm{D}_a/\mathrm{D}t$ is the objective time derivative, defined by

$$\frac{\mathrm{D}_a \underline{\underline{\tau}}}{\mathrm{D}t} = \left(\frac{\partial}{\partial t} + \underline{U} \cdot \nabla \right) \underline{\underline{\tau}} + \underline{\underline{\tau W}} - \underline{\underline{\tau W}} - a(\underline{\underline{D\tau}} - \underline{\underline{\tau D}})$$

where $\underline{\underline{W}} = \frac{1}{2}(\nabla \underline{U} - (\nabla \underline{U})^T)$ is the vorticity tensor; the parameter a satisfies $-1 \le a \le 1$.

The stress tensor $\underline{\underline{\tau}}$ can be conveniently decomposed in two parts as follows:

$$\underline{\underline{\tau}} = \underline{\underline{\tau^s}} + \underline{\underline{\tau^p}}$$

where $\underline{\underline{\tau^s}}$ and $\underline{\underline{\tau^p}}$ are the Newtonian and the non-Newtonian contributions to $\underline{\underline{\tau}}$ respectively, such that

$$\underline{\underline{\tau^s}} = 2\eta \frac{\lambda_2}{\lambda_1} \underline{\underline{D}} - P \cdot \underline{\underline{I}} = 2\eta_s \underline{\underline{D}} - P \cdot \underline{\underline{I}}$$

where $\underline{\underline{I}}$ is the unit tensor

$$\underline{\underline{\tau^p}} + \lambda_1 \frac{\mathrm{D}_a \underline{\underline{\tau^p}}}{\mathrm{D}t} = 2\eta \left(1 - \frac{\lambda_2}{\lambda_1} \right) \underline{\underline{D}} = 2\eta_p \underline{\underline{D}}$$

For simplicity we will denote $\underline{\underline{\tau^p}}$ by $\underline{\underline{\tau}}$.

For a two-dimensional system [18], the dimensionless steady state problem can be written as

$$\begin{cases}
\dfrac{\partial U}{\partial x} + \dfrac{\partial V}{\partial y} = 0 \\
\dfrac{\partial}{\partial x}\left(R_e UU - (1-w_r)\dfrac{\partial U}{\partial x} \right) + \dfrac{\partial}{\partial y}\left(R_e VU - (1-w_r)\dfrac{\partial U}{\partial y} \right) = -\dfrac{\partial P}{\partial x} + \dfrac{\partial \tau_{xx}}{\partial x} + \dfrac{\partial \tau_{xy}}{\partial y} \\
\dfrac{\partial}{\partial x}\left(R_e UV - (1-w_r)\dfrac{\partial V}{\partial x} \right) + \dfrac{\partial}{\partial y}\left(R_e VV - (1-w_r)\dfrac{\partial V}{\partial y} \right) = -\dfrac{\partial P}{\partial y} + \dfrac{\partial \tau_{yy}}{\partial y} + \dfrac{\partial \tau_{xy}}{\partial x} \\
\tau_{xx} + \dfrac{\partial}{\partial x}(W_e U \tau_{xx}) + \dfrac{\partial}{\partial y}(W_e V \tau_{xx}) = W_e\left(\dfrac{\partial U}{\partial y} - \dfrac{\partial V}{\partial x} \right)\tau_{xy} + 2aW_e \dfrac{\partial U}{\partial x}\tau_{xx} + aW_e\left(\dfrac{\partial U}{\partial y} + \dfrac{\partial V}{\partial x} \right)\tau_{xy} + 2w_r \dfrac{\partial U}{\partial x} \\
\tau_{yy} + \dfrac{\partial}{\partial x}(W_e U \tau_{yy}) + \dfrac{\partial}{\partial y}(W_e V \tau_{yy}) = W_e\left(\dfrac{\partial V}{\partial x} - \dfrac{\partial U}{\partial y} \right)\tau_{xy} + 2aW_e \dfrac{\partial V}{\partial y}\tau_{yy} + aW_e\left(\dfrac{\partial U}{\partial y} + \dfrac{\partial V}{\partial x} \right)\tau_{xy} + 2w_r \dfrac{\partial V}{\partial y} \\
\tau_{xy} + \dfrac{\partial}{\partial x}(W_e U \tau_{xy}) + \dfrac{\partial}{\partial y}(W_e V \tau_{xy}) = -\dfrac{1}{2} W_e(\tau_{xx} - \tau_{yy})\left(\dfrac{\partial U}{\partial y} - \dfrac{\partial V}{\partial x} \right) + w_r\left(\dfrac{\partial U}{\partial y} + \dfrac{\partial V}{\partial x} \right) + \dfrac{1}{2} aW_e(\tau_{xx} + \tau_{yy})\left(\dfrac{\partial U}{\partial y} + \dfrac{\partial V}{\partial x} \right)
\end{cases}$$

where U and V are the velocities components in the x- and y-directions respectively;

$$\underline{\underline{\tau}} = \begin{pmatrix} \tau_{xx} & \tau_{xy} \\ \tau_{xy} & \tau_{yy} \end{pmatrix}$$

$$R_e = \rho \frac{UL}{\eta}$$

is the Reynolds number

$$W_e = \lambda_1 \frac{U}{L}$$

is the Weissenberg number and $w_r = 1 - (\lambda_2/\lambda_1)$ (U and L represent a typical velocity and a typical length of the flow).

2.2. The boundary conditions

The fully developed Poiseuille flow is imposed at the inlet and outlet sections (see Figure 1)

Inlet section (Γ_m):

$$U(-L_m, y) = \frac{1}{8}\left(1 - \left(\frac{y}{4}\right)^2\right), \qquad V(-L_m, y) = 0$$

$$\tau_{xx}(-L_m, y) = 18 w_r W_e \left(\frac{U_m}{4}\right)^2 \left(\frac{y}{4}\right)^2, \qquad \tau_{yy}(-L_m, y) = 0$$

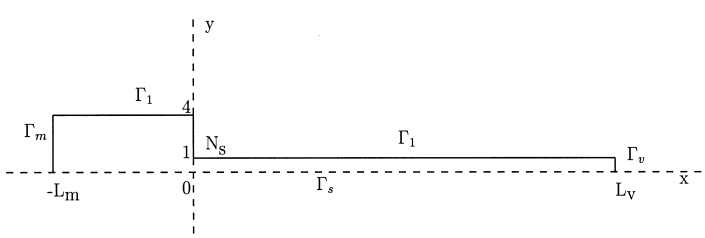

Figure 1. The 4:1 abrupt planar contraction ($L_m = 10.0$ and $L_v = 20.0$).

$$\tau_{xy}(-L_m, y) = -3w_r \frac{U_m}{4}\frac{y}{4}$$

Outlet section (Γ_v):

$$U(L_v, y) = \frac{1}{2}(1-y^2), \qquad V(L_v, y) = 0$$

Symmetry axis:

$$\frac{\partial U}{\partial y} = 0, \qquad V = 0 \quad \text{and} \quad \tau_{xy} = 0$$

Wall (Γ_1):

$$U = V = 0$$

3. NUMERICAL METHOD

All of the governing equations can be written as a general transport equation in the form

$$\text{div}(\Lambda U\Phi - \Gamma\nabla\Phi) = S_\Phi \tag{4}$$

where Φ is the primitive variable, the coefficients Γ and Λ have different meanings for different primitive variables, and S_Φ represents the source term. The definition of different variables can be found in Table I.

We use a staggered non-uniform grid system with pressure P, τ_{xx} and τ_{yy} given at the center of a cell, the components of the velocity given at the middle of the sides, and the component τ_{xy} of the stress given at the top of a cell (see Figure 2).

A finite volume formulation (FVF) is used as a discrete approximation to the continuity, momentum, and constitutive equations.

The flow domain is divided into a set of non-overlapping control volumes over which Equation (4) is integrated, and then the fluxes are approximated across the cell faces in terms of nodal values.

A control volume in two-dimensional space is determined by a quadrilateral surrounding a grid point (see Figure 3).

The subscript P refers to the grid point where the quantity is defined. The subscripts 'e', 'w', 's', and 'n' denote the control volume faces where the derivatives are evaluated using the central finite difference approximation.

The term S_Φ is generally assumed to be a linear function of variable Φ

$$S_\Phi = S_C + S_P\Phi_P$$

Table I. The definition of different variables.

Φ	Λ	Γ	S_Φ
1	1	0	0
U	R_e	$1-w_r$	$-\dfrac{\partial P}{\partial x}+\dfrac{\partial \tau_{xx}}{\partial x}+\dfrac{\partial \tau_{xy}}{\partial y}$
V	R_e	$1-w_r$	$-\dfrac{\partial P}{\partial y}+\dfrac{\partial \tau_{yy}}{\partial y}+\dfrac{\partial \tau_{xy}}{\partial x}$
τ_{xx}	W_e	0	$W_e\left(\dfrac{\partial U}{\partial y}-\dfrac{\partial V}{\partial x}\right)\tau_{xy}+2aW_e\dfrac{\partial U}{\partial x}\tau_{xx}+aW_e\left(\dfrac{\partial U}{\partial y}+\dfrac{\partial V}{\partial x}\right)\tau_{xy}+2w_r\dfrac{\partial U}{\partial x}-\tau_{xx}$
τ_{yy}	W_e	0	$-W_e\left(\dfrac{\partial U}{\partial y}-\dfrac{\partial V}{\partial x}\right)\tau_{xy}+2aW_e\dfrac{\partial V}{\partial y}\tau_{yy}+aW_e\left(\dfrac{\partial U}{\partial y}+\dfrac{\partial V}{\partial x}\right)\tau_{xy}+2w_r\dfrac{\partial V}{\partial y}-\tau_{yy}$
τ_{xy}	W_e	0	$-\dfrac{1}{2}W_e(\tau_{xx}-\tau_{yy})\left(\dfrac{\partial U}{\partial y}-\dfrac{\partial V}{\partial x}\right)+\dfrac{1}{2}aW_e(\tau_{xx}+\tau_{yy})\left(\dfrac{\partial U}{\partial y}-\dfrac{\partial V}{\partial x}\right)+w_\tau\left(\dfrac{\partial U}{\partial y}-\dfrac{\partial V}{\partial x}\right)-\tau_{xy}$

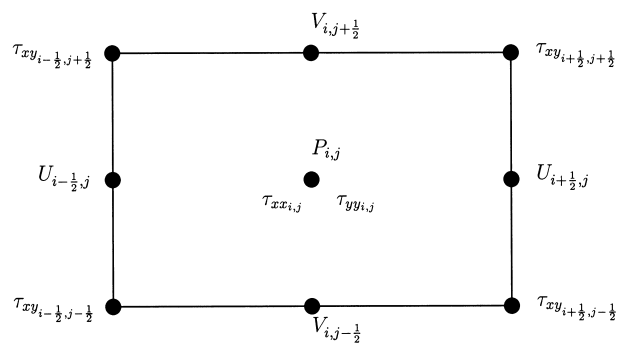

Figure 2. Pressure, velocity, and stress tensor in the cell (i, j).

where S_C is the part of S_Φ that does not explicitly depend on Φ and S_P is the coefficient of Φ_P which is made negative to enhance the numerical stability of the discretized equation (see Reference [14]). The resulting integrated equation is written in pseudo-linear form

$$A_P\Phi_P=\sum_m A_m\Phi_m+b_P$$

where the index m runs over the nodal points W, E, N, S

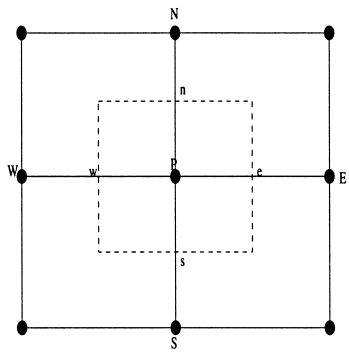

Figure 3. The control volume for grid point P.

$$b_P = S_C \Delta V$$

$$A_i = D_i f(|Pe_i|) + \max(\text{sign}(i) F_i, 0)$$

$$A_P = \sum_m A_m - S_P \Delta V$$

where ΔV is the control volume magnitude; Pe_i is the local Peclet number defined by $Pe_i = F_i/D_i$, while $f(|Pe_i|)$, $i \in \{\text{e, w, n, s}\}$, is a function of the discretization scheme, F_i is the mass flux through the corresponding face normal to the i-direction of control volume; D_i is the local diffusion conductance. sign(i) is $+1$ for $i \in \{\text{w, s}\}$ and -1 for $i \in \{\text{e, n}\}$.

In our calculations, the hybrid scheme is used in the momentum equations

$$f(|Pe_i|) = \max\left(0,\ 1 - \frac{|Pe_i|}{2}\right)$$

while the upwind scheme is used in the constitutive equations for the stresses

$$f(|Pe_i|) = 1$$

Linearization is performed by evaluating the coefficients using velocities from the previous iteration.

3.1. Solution algorithm

The discretized equations for each control volume in the computational domain consist of a set of linear algebraic equations that can be solved easily by means of the symmetrical coupled Gauss–Seidel (SCGS) smoothing procedure.

For viscoelastic fluid flow computations, the extra stress is non-linearly coupled via the source term of the momentum equations. Here, the decoupled technique can be adopted in such a way that the source term and the stress is updated by solving the discretized constitutive equations for after obtaining the kinematics field from the momentum equations.

To obtain the kinematic fields an equation for the pressure is obviously necessary because it is also an unknown. The strategy of pressure correction (SIMPLE) is used to produce the pressure equation in which the continuity of the field is enforced via a pressure correction, so that the resulting pressure relation, which couples the pressure and the velocities, replaces the continuity relation, while the momentum equations retain their role for determining the velocity field. As shown in Figure 3, for the P-centered control volume for scalar fields, the velocities $\underline{U}_i$ $(i = x, y)$ are discretized using their values on the faces normal to the i-direction. Thus, the location of the control volume for $\underline{U}_i$ in the momentum equations is staggered only in the i-direction relative to the control volume for the fields.

The steps of present algorithm are as follows:

1. Compute the velocities.
2. Compute the pressure and correct the velocities.
3. Compute the stress.

4. MULTIGRID METHOD

The problem can be symbolized by: find $(\underline{U}, P, \underline{\underline{\tau}})$ solution of

$$L(\underline{U}, P, \underline{\underline{\tau}}) = 0 \quad \text{in } \Omega \tag{5}$$

where L is a non-linear operator.

After discretization of Equation (5), we get a non-linear dimensional operator L_n, which satisfies

$$L_n(\underline{U_n}, P_n, \underline{\underline{\tau_n}}) = b_n$$

In order to solve this problem we use a FAS multigrid algorithm (see Brandt [16] and Hackbusch [17]).

Let $(\Omega_k)_{1 \leq k \leq n}$ be a set of n grids of domain Ω, Ω_n is the finest grid and Ω_1 is the coarsest grid. For $k = 1, \ldots, n$, let L_k be a non-linear finite-dimensional operator approximation of L on the grid Ω_k. We denote by $(\underline{U}_k, P_k, \underline{\underline{\tau}}_k)$ an approximation of $(\underline{U}, P, \underline{\underline{\tau}})$ on the grid Ω_k. $\mathscr{E}_k^{k+1}$ denotes the extension operator from grid Ω_k to grid Ω_{k+1} an $\mathscr{R}_k^{k-1}$ is the projection operator from grid Ω_k to grid Ω_{k-1}.

On each grid we solve

$$L_k(\underline{U}_k, P_k, \underline{\tau}_k) = b_k \tag{6}$$

by a relaxation procedure $\mathscr{M}_k$ and we denote by $\mathscr{R}_k^m(\underline{U}_k^{(1)}, P_k^{(1)}, \underline{\tau}_k^{(1)})$ the vector obtained after m iterations with the initial vector $(\underline{U}_k^{(1)}, P_k^{(1)}, \underline{\tau}_k^{(1)})$. The object of the FAS algorithm is to solve

$$L_n(\underline{U}_n, P_n, \underline{\tau}_n) = 0 \tag{7}$$

on the finest grid Ω_n by solving intermediate problems (6) on coarser grids in order to reduce the number of iterations on the finest grid.

FAS algotithm

{0} $(\underline{U}_n, P_n, \underline{\tau}_n)$ initial approximation of solution of Equation (7)
{1} $k := n$
{2} $(\underline{U}_k, P_k, \underline{\tau}_k) = \mathscr{M}_k^{m_k}(\underline{U}_k, P_k, \underline{\tau}_k)$ (m_k iterations of relaxation on grid Ω_k)
{3} Compute $b_{k-1} = \mathscr{R}_k^{k-1}(b_k - L_k(\underline{U}_k, P_k, \underline{\tau})) + L_{k-1}(\mathscr{R}_k^{k-1}(\underline{U}_k, P_k, \underline{\tau}_k))(\underline{U}_{k-1}, P_{k-1}, \underline{\tau}_{k-1}) = \mathscr{R}_k^{k-1}(\underline{U}_k, P_k, \underline{\tau}_k)$ (initializing of solution on grid Ω_{k-1}) $k := k-1$ (crossing to the coarser grid)
{4} If $k > 1$, go to {2}
Else $(\underline{U}_1, P_1, \underline{\tau}_1) = \mathscr{M}_1^{m_1}(\underline{U}_1, P_1, \underline{\tau}_1)$ (m_1 iterations of relaxation on the coarsest grid Ω_1)
{5} Correct the approximation obtained on Ω_{k+1} with the extension of $((\underline{U}_k, P_k, \underline{\tau}_k) - \mathscr{R}_{k+1}^k(\underline{U}_{k+1}, P_{k+1}, \underline{\tau}_{k+1}))$

$$(\underline{U}_{k+1}, P_{k+1}, \underline{\tau}_{k+1}) = (\underline{U}_{k+1}, P_{k+1}, \underline{\tau}_{k+1}) + \mathscr{E}_k^{k+1}((\underline{U}_k, P_k, \underline{\tau}_k) - \mathscr{R}_{k+1}^k(\underline{U}_{k+1}, P_{k+1}, \underline{\tau}_{k+1}))$$

$k := k+1$ (crossing to the finer grid)
{6} $(\underline{U}_k, P_k, \underline{\tau}_k) = \mathscr{M}_k^{\mu_k}(\underline{U}_k, P_k, \underline{\tau}_k)$ (μ_k iterations of relaxation on grid Ω_k)
{7} If $k < n$, go to {5}
Else convergence test
If convergence done, good, end
Else go to {2}

In practice for the FAS procedure we take $m_1 = 10$, $\mu_k = 3$, and $m_k = 2$ $(k = 2, \ldots, n)$ for small Weissenberg numbers and $m_1 = 50$, $\mu_k = 20$ and $m_k = 20$ $(k = 2, \ldots, n)$ for large Weissenberg numbers.

The operators $\mathscr{R}_k^{k+1}$ and $\mathscr{E}_k^{k+1}$ represent a tiny part of the CPU time, so we can take good interpolations in order to decrease the number of global iterations of the finest grid. For more details on these operators, the reader is referred to Reference [18].

4.1. Resolution on one grid: decoupled formulation

In this section we see how to solve system (6) on each grid Ω_k. This system is obtained by discretizing problem (5) on grid Ω_k.

On each grid Ω_k we decompose system (6) as follows:

$$L_k^1(\underline{U}_k, P_k, \underline{\underline{\tau}}_k) = b_k^1 \tag{8}$$

$$L_k^2(\underline{U}_k, P_k, \underline{\underline{\tau}}_k) = b_k^2 \tag{9}$$

Equation (8) presents the discretization of the momentum and continuity equation and boundary conditions for $\underline{U}$. The unknown variables are velocity and pressure. The stress tensor is a known datum of problem (8).

Equation (9) presents the discretization of the constitutive equation and the boundary conditions for $\underline{\underline{\tau}}$. The unknown variable is the stress tensor and the velocity field is known. To solve Equation (7), we execute m_k iterations in the following method:

Step 1: At the first iteration, $\underline{\underline{\tau}}_k$ is initialized on grid Ω_k, in the following iterations, $\underline{\underline{\tau}}_k$ is given by Step 2 of the previous iteration. We take this value of $\underline{\underline{\tau}}_k$ in Equation (8), which we solve by executing a number, *itvit*, of equilibrium and continuity iterations.

Step 2: We take back the values of $\underline{U}_k$ obtained in Step 1 for Equation (9), which we solve by executing a number, *itcont*, of stress tensor iterations.

The numerical experiences have shown that we must choose *itvit* larger than *itcont* to ensure the stability of the method. In numerical tests we have taken $invit = 5$ or 10 and $itcont = 1$.

5. NUMERICAL RESULTS

The algorithm developed here is tested on the benchmark problem: the 4:1 contraction problem. The difficulty of this problem comes from the geometric singularity at the re-entrant corner. Most previous numerical simulations for this problem encountered an upper limit of W_e that decreases with increasing mesh resolution. Four different meshes depicted in Figures 4–7 are considered for the study. They have in common entry and exit lengths equal to 10 and 20 radii respectively ($L_m = 10$, $L_v = 20$). They are assumed to be sufficiently long so that the fully developed velocity and stress profiles are at the inlet and outlet boundaries. For a further visualization we have reported on the grids just in the vicinity of the corner, with $x \in [-4, 4]$. Very thin cells were required around the re-entrant section to account for the large stress that develops in the vicinity of the corner. Table II gives the total number of nodes (NN) and the area (Area) of the cells adjacent to the re-entrant corner for each grid.

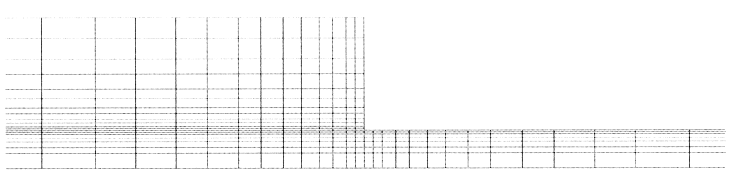

Figure 4. Mesh 1.

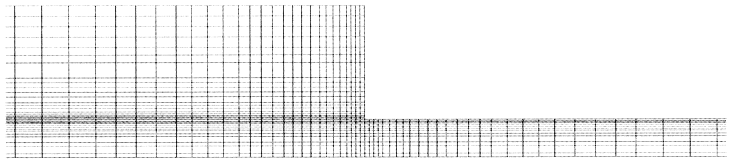

Figure 5. Mesh 2.

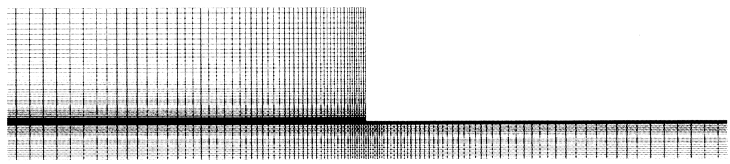

Figure 6. Mesh 3.

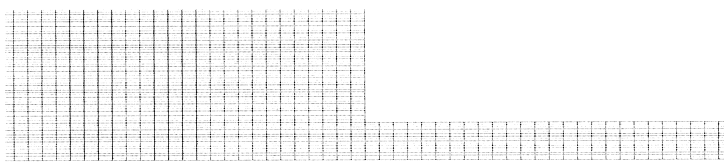

Figure 7. Mesh 4.

Table II. The NN and the area for each grid

	NN	Area
Mesh 1	624	5×10^{-3}
Mesh 2	2496	1.25×10^{-3}
Mesh 3	9984	3.125×10^{-4}
Mesh 4	6144	9.76×10^{-3}

To test the convergence of the simulations with mesh refinement, we plot profiles of the first normal stress difference ($\tau_{xx}-\tau_{yy}$) along the centerline (Figure 8). It is clear that, when compared with Meshes 1 and 3, Mesh 2 allows good convergence; and we will limit the present simulation to this grid. Table III gives the time CPU reclaimed by each grid with both the single grid and the multigrid algorithm. This table shows that if we use the multigrid algorithm, we can simulate the 4:1 contraction problem in a short time by using a very thin mesh.

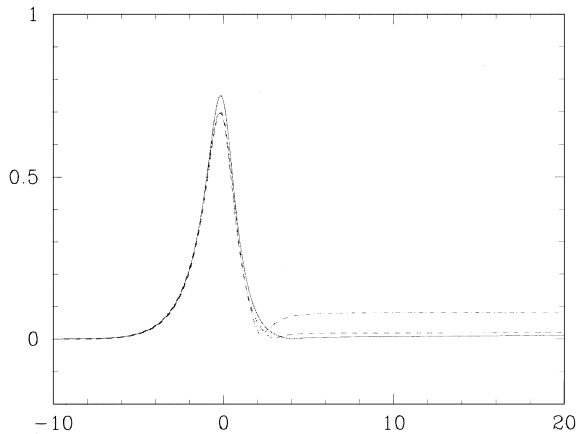

Figure 8. Profiles of $(\tau_{xx} - \tau_{yy})$ on $y = 1$: – · – · –, Mesh 1; – – –, Mesh 2; —, Mesh 3.

Table III. The CPU of each mesh, $W_e = 1.5$.

CPU	Mesh 1	Mesh 2	Mesh 3	Mesh 4
Single grid	1 min 11 s	5 min 20 s	24 min 12 s	10 min 29 s
Multigrid	49 s	2 min 16 s	6 min 42 s	3 min 41 s

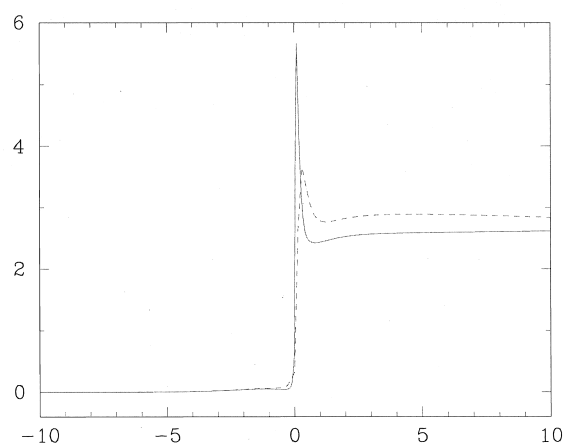

Figure 9. Profiles of τ_{xx} on $y = 1$: – – –, Mesh 2; —, Mesh 4.

To validate the use of non-uniform grid we plot profiles of τ_{xx} and τ_{yy} along the axis $y = 1$ (Figures 9 and 10) using Meshes 4 and 2. These figures show that if we use a non-uniform grid, we can simulate the 4:1 contraction with a small number of nodes and very thin cells around the re-entrant corner.

The flow along the centerline has an elongation nature, and the elongational properties of the rheological models play an important role in determining the way it responds to the accelerating forces when it approaches the corner. Velocity components profiles for Weissenberg number $W_e = 4.5$ are plotted in Figure 11. This figure shows an important velocity overshoot near the corner.

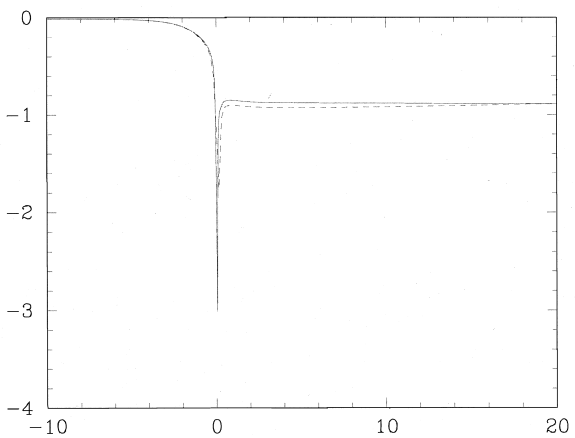

Figure 10. Profiles of τ_{xy} on $y = 1$: —, Mesh 2; – – –, Mesh 4.

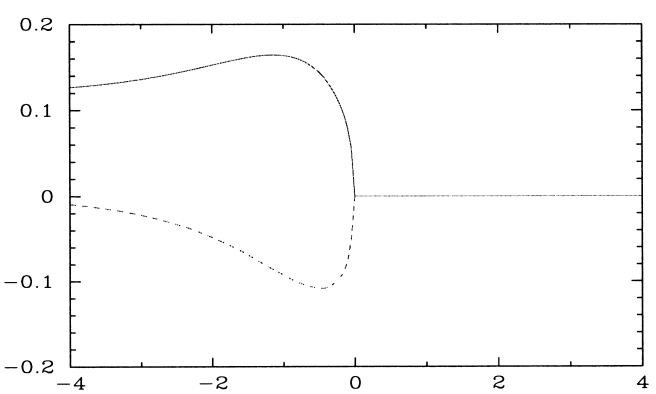

Figure 11. Velocity components profiles: —, U; – – –, V.

First normal stress difference profiles for different value of the Weissenberg number are reproduced in Figure 12. The maximum of $(\tau_{xx} - \tau_{yy})$ is reached just upstream of the entry section. As W_e increases, the value of this maximum increases sharply and the domain must be long enough.

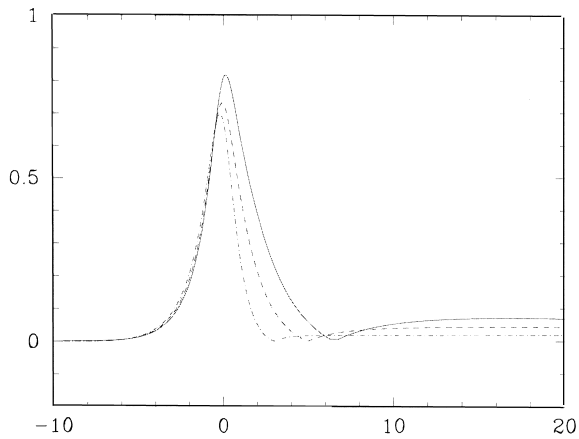

Figure 12. First normal stress difference: —, $W_e = 4.5$; – – –, $W_e = 3$; – · – · –, $W_e = 1.5$.

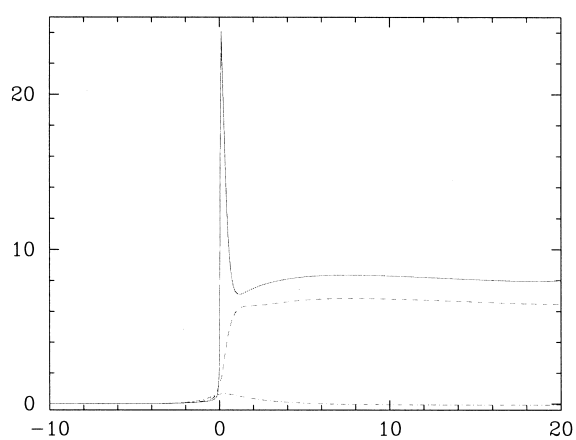

Figure 13. Profiles of τ_{xx} on $y = 0$, – · – · –; $y = 0.9$, – – –; $y = 1$, —; with $W_e = 4.5$.

Profiles of the normal extra-stress τ_{xx} as well as τ_{yy} are presented in Figures 13 and 14 for different values of y. We notice that when y increases, τ_{xx} and τ_{yy} peaks increase dramatically. The τ_{xx} and τ_{yy} profiles, on $y = 1$, for different values of W_e are reproduced in Figures 15 and 16. We notice that as W_e increases, the value of the maximum increases.

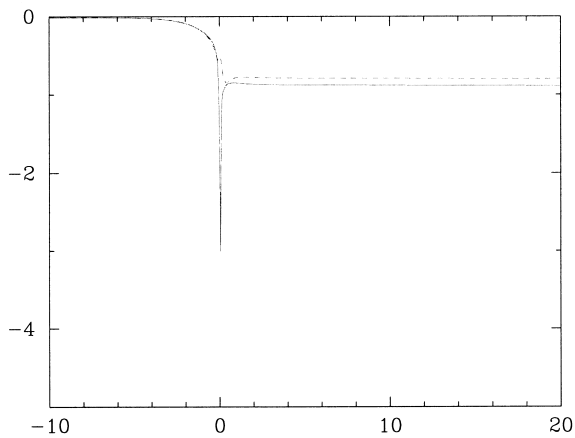

Figure 14. Profiles of τ_{xx} on $y = 0.9$, – – –; $y = 1$, —; with $We = 1.5$.

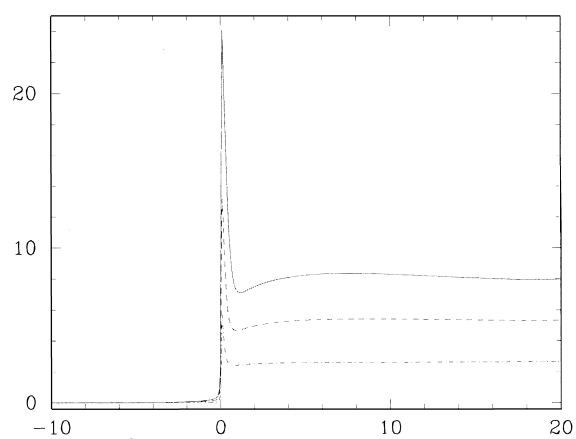

Figure 15. Profiles of τ_{xx}: – · – · –, $W_e = 1.5$; – – –, $W_e = 3$; —, $W_e = 4.5$.

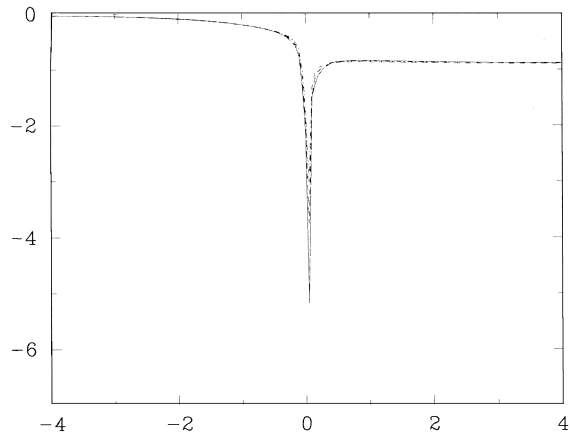

Figure 16. Profiles of τ_{xx}: $- \cdot - \cdot -$, $W_e = 1$; $- - -$, $W_e = 2$; —, $W_e = 3$.

In Figures 17 and 18 the pressure and streamline distributions are shown for $(R_e, w_r, W_e) = (0.1, 0.89, 4.5)$, where the solution becomes more and more oscillatory near re-entrant corner as W_e increases. In Figures 19 and 20 we present the distributions of τ_{xx} and τ_{yy} for $(R_e, w_r, W_e) = (0.1, 0.89, 4.5)$. It is clear that the re-entrant corner represents a singularity; many lines pass across this point.

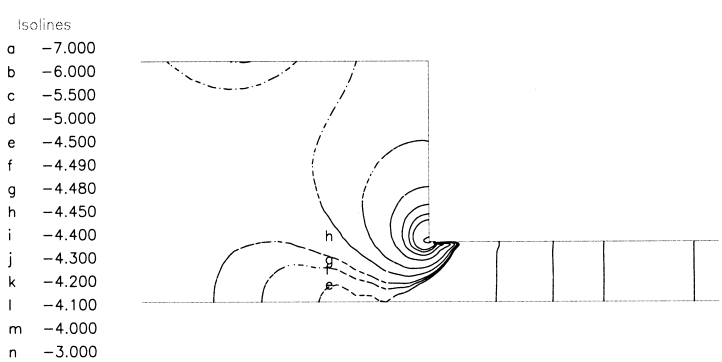

Figure 17. Isolines of pressure.

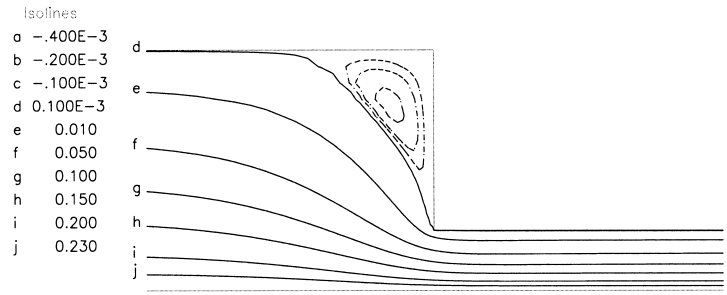

Figure 18. Isolines of streamline function.

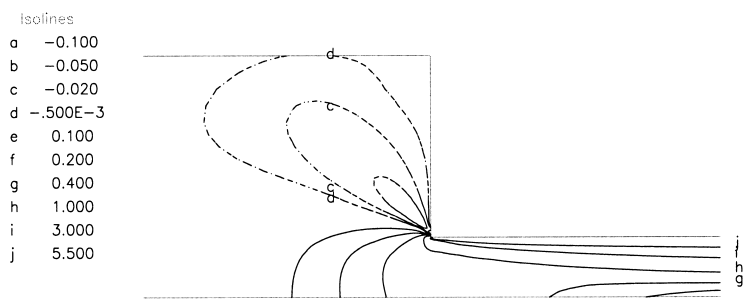

Figure 19. Isolines of τ_{xx}.

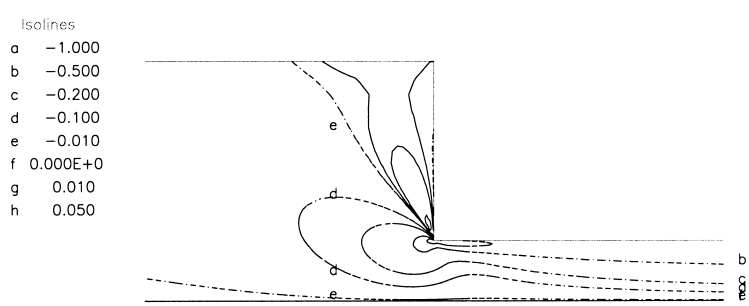

Figure 20. Isolines of τ_{xy}.

6. CONCLUSION

The planar 4:1 contraction flow of an Oldroyd-B fluid has been simulated by using a FVM with the FAS multigrid algorithm on a non-uniform staggered grid. The conservative and constitutive equations are solved using the FVM with a hybrid scheme for the velocities and first-order upwind approximation for the viscoelastic stresses. The iterative SIMPLE algorithm is employed to relax the coupled momentum and continuity equations. The non-linear algebraic equations over the flow domain are solved iteratively by the SCGS method. The solutions show that at high Weissenberg number, the domain must be long enough and the mesh must be thin enough. As a result, the FVM with FAS algorithm have allowed us to reproduce a stable and smooth solution on a very thin mesh with a small time CPU.

REFERENCES

1. Crochet MJ, Davies AR, Walters K. *Numerical Simulation of Non-Newtonian Flow*. Elsevier: Amsterdam, 1984.
2. Crochet MJ, Pilot G. Plane flow of fluid of second grate through a contraction. *Journal of Non-Newtonian Fluid Mechanics* 1976; **1**: 247–258.
3. Marchal JM, Crochet MJ. A new mixed finite elements for calculating viscoelastic flows. *Journal of Non-Newtonian Fluid Mechanics* 1987; **26**: 77–114.
4. King RC, Apelian MR, Armstrong RC, Brown RA. Numerically stable finite elements techniques for viscoelastic calculations in smooth and singular geometries. *Journal of Non-Newtonian Fluid Mechanics* 1988; **29**: 147–216.
5. Bindette S, Coates PJ, Armstrong RC, Brown RA. *Journal of Non-Newtonian Fluid Mechanics* 1989; **33**: 1–23.
6. Beris AN, Armstrong RC, Brown RA. Spectral/finite element calculation of the flow of a Maxwell fluid between eccentric rotating cylinders. *Journal of Non-Newtonian Fluid Mechanics* 1987; **22**: 129–167.
7. Rajagopalan D, Armstrong RC, Brown RA. Finite element methods for calculation of steady viscoelastic flow using constitutive equations with a Newtonian viscosity. *Journal of Non-Newtonian Fluid Mechanics* 1990; **36**: 159–192.
8. Fortin A, Zine A. An improved GMRES methods for solving viscoelastic fluid flow problems. *Journal of Non-Newtonian Fluid Mechanics* 1992; **42**: 1–18.
9. Fortin A, Fortin M. A new approach for the FEM simulation of viscoelastic flows. *International Journal for Numerical Methods in Fluids* 1989; **7**: 295–310.
10. Fortin A, Fortin M. A preconditioned generalized minimal residual algorithm for the numerical solution of viscoelastic fluid flows. *Journal of Non-Newtonian Fluid Mechanics* 1990; **36**: 227–288.
11. Hu HH, Joseph DD. Numerical simulation of viscoelastic flow past a cylinder. *Journal of Non-Newtonian Fluid Mechanics* 1990; **37**: 347–377.
12. Yoo JY, Na Y. A numerical study of the planar contraction flow of viscoelastic fluid using SIMPLER algorithm. *Journal of Non-Newtonian Fluid Mechanics* 1991; **39**: 89–106.
13. Darwich MS, Whiteman JR, Beris MJ. Numerical modelling of viscoelastic liquids using a finite volume method. *Journal of Non-Newtonian Fluid Mechanics* 1992; **45**: 311–337.
14. Sasmal GP. A finite volume approach for calculation of viscoelastic flow through an abrupt axisymmetric contraction. *Journal of Non-Newtonian Fluid Mechanics* 1995; **47**: 15–47.
15. Raghay S, Hakim A. Numerical simulation of White–Metzner fluid in a 4:1 contraction. *International Journal for Numerical Methods in Fluids* 2001; **35**: 559–573.
16. Brandt A. Multi-level adaptive solutions to boundary value problems. *Mathematics and Computers* 1977; **31**: 333–390.
17. Hackbusch W. *Multi-Grid Methods and Applications*. Springer: Berlin, 1985.
18. Almoatassime H. Simulation numérique des écoulements de fluides non Newtoniens par une méthode multigrille. Thèse, Université Paris XI Orsay, 1993.

